Advanced Composite Materials
Publication details, including instructions for authors and subscription information:
http://www.tandfonline.com/loi/tacm20

Fabrication method and compressive properties of CFRP isogrid cylindrical shells

Kazuhiro Sakata [a] & Goichi Ben [a]

[a] Department of Mechanical Engineering, College of Industrial Technology, Nihon University, 1-2-1, Izumicho, Narashino, Chiba, 275-8575, Japan

Version of record first published: 12 Nov 2012.

To cite this article: Kazuhiro Sakata & Goichi Ben (2012): Fabrication method and compressive properties of CFRP isogrid cylindrical shells, Advanced Composite Materials, 21:5-6, 445-457

To link to this article: http://dx.doi.org/10.1080/09243046.2012.743711

Advanced Composite Materials
Vol. 21, Nos. 5–6, October–December 2012, 445–457

Fabrication method and compressive properties of CFRP isogrid cylindrical shells

Kazuhiro Sakata* and Goichi Ben

Department of Mechanical Engineering, College of Industrial Technology, Nihon University, 1-2-1, Izumicho, Narashino, Chiba 275-8575, Japan

(*Received 23 February 2012; accepted 26 July 2012*)

Since isogrid structures are composed of triangular grid stiffeners and a surface skin, they have a high specific strength and stiffness. These structures are now being mainly used for aerospace applications. In order to produce a metal isogrid cylindrical shell, most of the thick metal plates must be cut off while the remaining thin surface skins with the stiffeners and both ends of the skins are welded to each other. This process needs a long lead time and a high cost, and unstable behaviors are observed in the joint parts. On the other hand, carbon fiber reinforced plastics (CFRP) isogrid cylindrical shells can be fabricated with an integral method by using a filament winding apparatus. In this study, a fabrication method of the CFRP isogrid cylindrical shells is proposed and their compressive tests are carried out to investigate the reinforcement effect of the grids on the CFRP isogrid cylindrical shells. Furthermore, the results of the static compressive tests are compared with numerical ones obtained by finite element method (FEM).

Keywords: CFRP cylindrical shell; isogrid structure; fabrication method; filament winding; compressive property; FEM

1. Introduction

Conventional isogrid stiffened cylindrical shells are composed of a thin surface skin shell and repetitive equilateral triangular grid stiffeners and they demonstrate a higher strength and stiffness due to their lightweight. Metallic isogrid structures are now used in the aerospace field such as in launch vehicles, payload fairings, engine ductings, and space station modules. In order to produce them, most of the thick metal plates must be cut off while the remaining thin surface skins with the stiffeners and both ends of the skins are welded to each other [1]. This process needs a long lead time and a high cost, and unstable strength of the joint parts is observed. On the other hand, some composite grid-stiffened structures were developed [2–7] and an automatic fiber placement machine was usually used for laminating structures having complex geometries [8,9]. In this study, we developed a fabrication method of the carbon fiber reinforced plastics (CFRP) isogrid cylindrical shells by using a three-axes filament winding apparatus and a silicone rubber mold. Moreover, their static compressive tests were carried out and the results of the static compressive tests were compared with numerical ones obtained by a finite element method (FEM) code of ANSYS.

*Corresponding author. Email: sakata.kazuhiro@nihon-u.ac.jp

ISSN 0924-3046 print/ISSN 1568-5519 online

http://dx.doi.org/10.1080/09243046.2012.743711
http://www.tandfonline.com

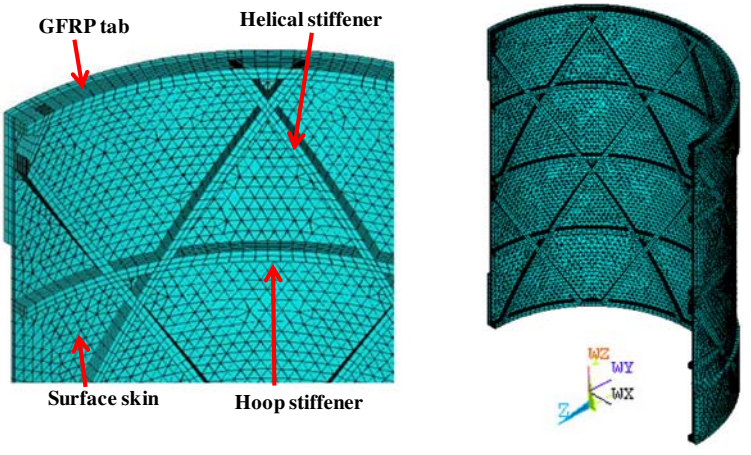

Figure 1. FEM model of the CFRP isogrid cylindrical shell.

2. Numerical analysis

In order to verify the reinforcement effect of the grids on the CFRP isogrid cylindrical shells, the numerical analysis by using the ANSYS code was carried out. Figure 1 shows a half symmetrical model of the CFRP isogrid cylindrical shell. The winding angles of the surface skin layers were ± 60° (helical winding) or 90° (hoop winding). The surface skin layers and the stiffeners consisted of two plies and six plies, respectively. The linear bucking load of the two cylindrical shells without the grids (hereafter called as the 'without grid 60' and the 'without grid 90') and the two isogrid cylindrical shells with the grids (hereafter called as the 'with grid 60' and the 'with grid 90') were calculated. The four-node finite strain shell elements were used. In the models of the 'without grid 60' and the 'without grid 90', the total number of nodes were 2829 and the total number of elements were 2720. In the 'with grid 60' and the 'with grid 90'

Table 1. Material properties.

CFRP	
Modulus of elasticity	
Longitudinal	129 GPa
Transverse	9.3 GPa
Shear	4.2 GPa
Poisson ratio	
Longitudinal	0.32
Transverse	0.02
Compressive strength	
Longitudinal	1570 MPa
Transverse	190 MPa
Shear	140 MPa
GFRP	
Modulus of elasticity	
Longitudinal	12 GPa
Transverse	12 GPa
Shear	2.5 GPa
Poisson ratio	
Longitudinal	0.30
Transverse	0.30

Table 2. Dimensions of the specimens.

	Without grid		With grid		
	Without grid 60	Without grid 90	With grid 60	With grid 90	Grid alone
Winding angle of skin	±60°	90°	±60°	90°	—
Shell length (mm)	138.4	139.0	135.1	137.5	137.8
Diameter (mm)	110.4	110.0	110.8	108.5	106.3
Plate thickness (mm)	0.7	0.9	0.6	0.8	—
Stiffener width (mm)	—	—	2.2	2.0	2.3
Stiffener height (mm)	—	—	3.2	2.5	2.0
Weight (N)	0.757	0.767	1.04	1.06	0.265

Table 3. FEM results of linear buckling load.

	Without grid		With grid	
FEM model	60	90	60	90
Linear buckling load (kN)	35.8	34.3	86.6	109.3

models, the total number of nodes were 7326 and 8371, respectively, and the total number of elements were 12,200 and 14,108, respectively. Tables 1 and 2 list the material properties and the geometries of the CFRP isogrid cylindrical shells with or without the grids, and the isogrid stiffened shell without the surface layer (hereafter called as the 'grid alone'). These values were obtained from the average values of three specimens for the each case in the experiments. Table 3 shows the FEM results of the linear buckling loads. The linear buckling loads of the 'with grid 60' and the 'with grid 90' models were 2.4 and 3.2 times larger than those of the 'without grid 60' and the 'without grid 90' models, respectively. Figures 2 and 3 show the buckling modes of the 'with grid 60' and the 'with grid 90' models. Although the large buckling deformation occurred in the 'with grid 90' model (Figure 3), the local buckling took place at the surface skin parts surrounded the grids in the 'with grid 60' model (Figure 2).

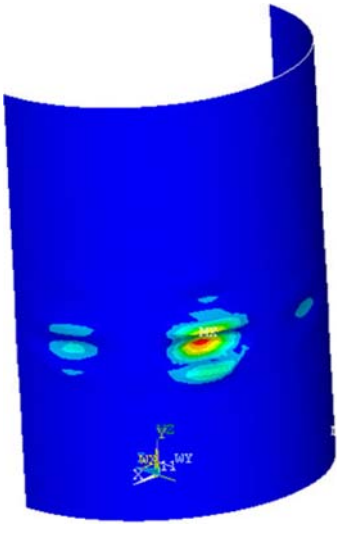

Figure 2. FEM result of the 'with grid 60' model.

Figure 3. FEM result of the 'with grid 90' model.

3. Fabrication of the CFRP isogrid cylindrical shells

3.1. Silicone rubber mold

Three grooves having 0 (horizontal direction) and ± 60° directions were cut on the surface of the thick aluminum plate of 193 mm in width and 314 mm in length and the horizontal groove was shifted to avoid the intersection of three grooves at the same point (Figure 4) [10,11]. These points are called the offset points.

Next, plastic bars of 2 mm in width and 6 mm in height were inserted into the grooves of the metallic female mold after which the metallic female mold becomes the metallic male mold (Figure 5).

Finally, in order to obtain the silicone rubber female mold, liquid silicone rubber was infused to the metallic male mold, as shown in Figure 5 and then it was cured under the room temperature.

Since the outer diameter of the mandrel in the filament winding apparatus was 90 mm, the four silicone rubber female molds were bonded each other, as shown in Figure 6. Even if the

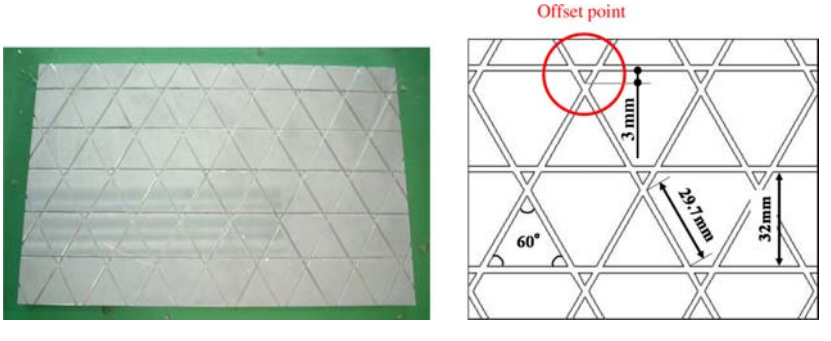

Figure 4. Metallic female mold.

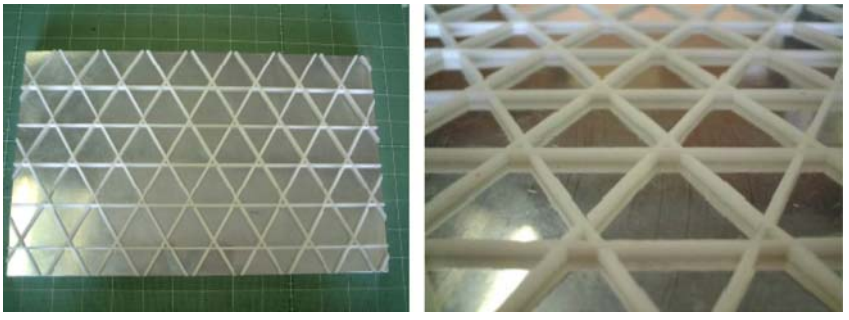

Figure 5. Metallic male mold.

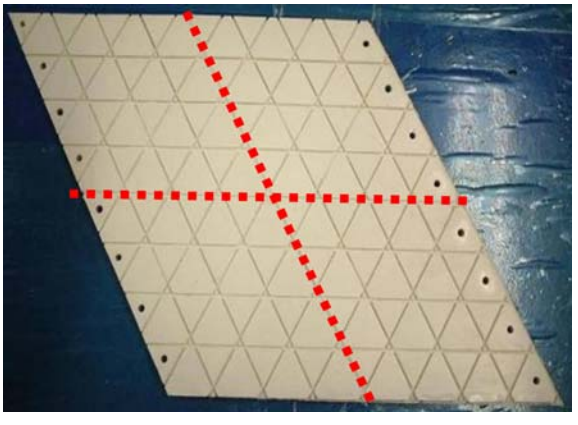

Figure 6. Silicone rubber female mold.

mandrel diameters changed, these silicone rubber female molds can be adapted by increasing or decreasing their number. When the CFRP isogrid cylindrical shell was fabricated with the rectangle-shaped silicone rubber female mold, as shown in Figure 7, a seam line arouse and this line gave the irregularity of the surface shape of the CFRP isogrid cylindrical shell (Figure 8). On the other hand, when the parallelogram-shaped female mold (Figure 9) was wound around the mandrel, the seam line was in accord with one of the helical directions. Therefore, the paral-

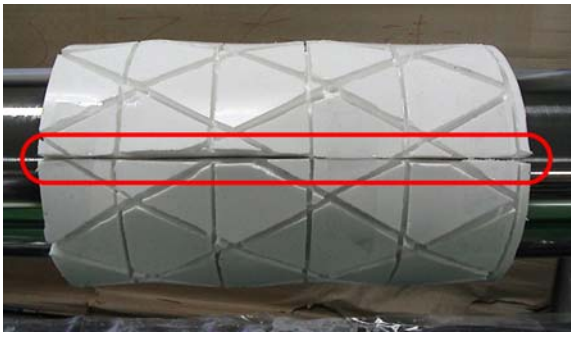

Figure 7. Rectangle-shaped silicone rubber female mold.

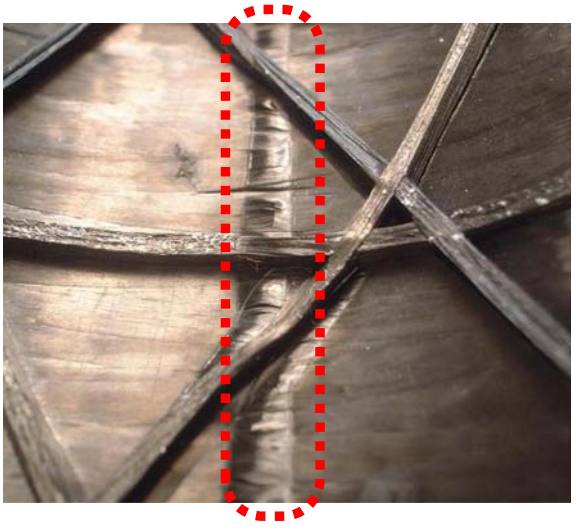

Figure 8. CFRP isogrid cylindrical shell fabricated by using the rectangle-shaped silicone rubber female mold.

Figure 9. Parallelogram-shaped silicone rubber female mold.

lelogram-shaped female mold was better than the rectangular-shaped silicone rubber female mold with regard to the surface accuracy of the CFRP isogrid cylindrical shells.

3.2. Filament winding process

The CFRP isogrid cylindrical shell was fabricated by the three-axes filament winding apparatus. First, the silicone rubber female mold was wound around the mandrel of the filament winding apparatus. The bolts were used to join the mandrel and the silicone rubber female mold. In order to guide the fibers during the winding process, some number of pins were set on both sides of the mandrel (Figure 10).

Next, the grooves of the isogrid stiffener parts were buried with six plies of the carbon fiber tow prepregs. Their winding angles were $\pm 30°$ for the helical stiffeners and 90°for the hoop stiffeners, respectively (Figure 11).

After finishing the fabrication of the isogrid stiffeners, the bolts were removed from the female mold and then the surface skin layers were wound with the carbon fiber tow prepregs on the female mold and the isogrid stiffener parts. The surface skin consisted of two plies

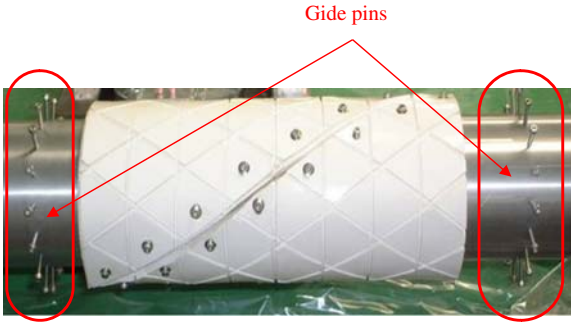

Figure 10. Female mold and guide pins set on the mandrel.

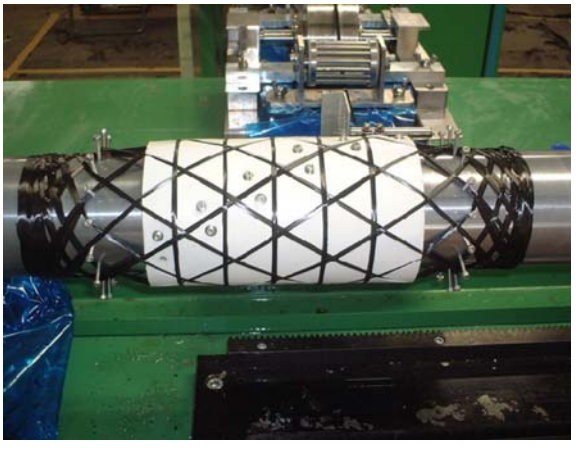

Figure 11. Filament winding process for the isogrid stiffener parts.

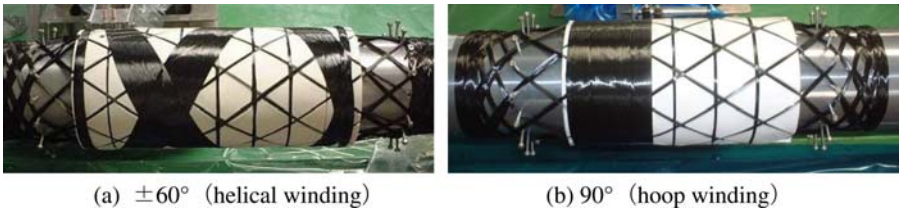

(a) ±60° (helical winding) (b) 90° (hoop winding)

Figure 12. Filament winding process for the surface skin layers.

and the winding angles of the 'with grid 60' and the 'with grid 90' were ± 60° or 90° (Figure 12) and they were cured for one hour at 130 °C.

After curing, the CFRP isogrid cylindrical shell was removed from the mandrel and then the silicone rubber female mold was removed from the inside of the CFRP isogrid cylindrical shell.

Table 2 lists the average dimensions of the isogrid CFRP cylindrical shells. In order to verify the reinforcement effect of the grids on the CFRP isogrid cylindrical shells, the CFRP cylindrical shells without grids and the isogrid stiffener shells without surface skin layer were also fabricated.

4. Axial compressive tests

4.1. Experimental results

In order to prevent fractures at the edges of the specimens, the glass fiber reinforced plastics (GFRP) were wound on both the edges of the specimens and the axial compressive tests were carried out with the speed of 0.5 mm/min. Figures 13–15 show the load to the displacement

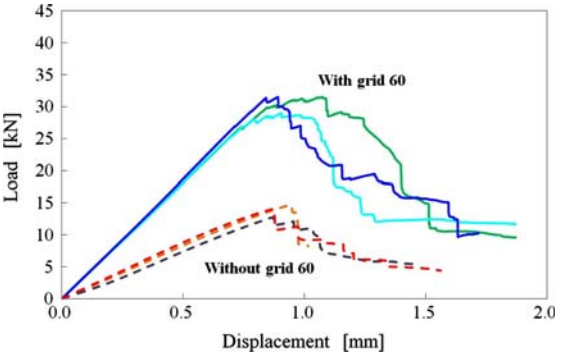

Figure 13. Load–displacement curves of the ‘without grid 60’ and the ‘with grid 60’ specimens.

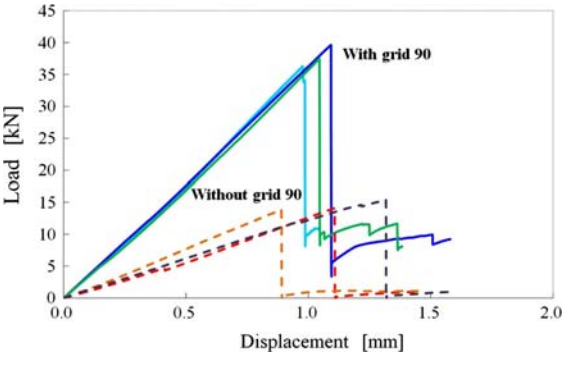

Figure 14. Load–displacement curves of the ‘without grid 90’ and the ‘with grid 90’ specimens.

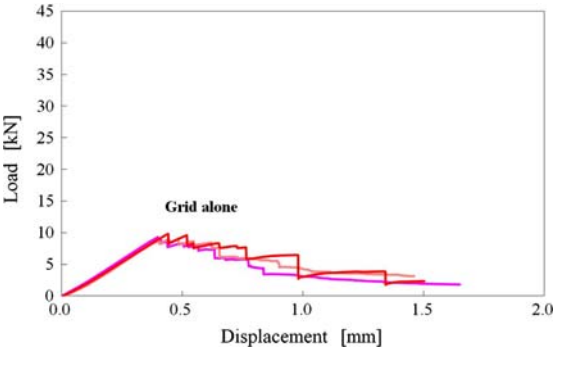

Figure 15. Load–displacement curves of the ‘grid alone’ specimens.

Table 4. Average maximum loads.

Angle of surface skin	Grid alone (kN)	Without grid (kN)	With grid (kN)
±60	9.6	13.9	30.7
90		14.5	37.8

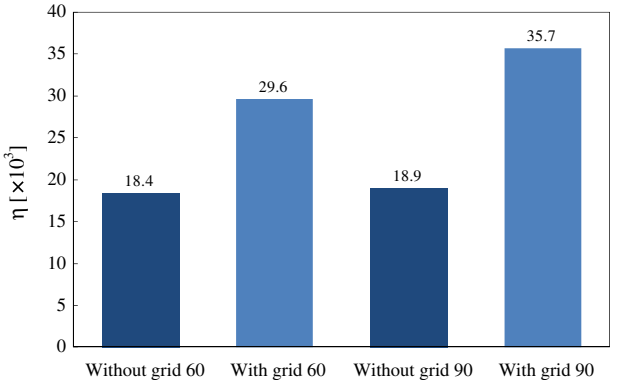

Figure 16. Specific strength of the 'without grid' and the 'with grid' specimens.

curves of every specimen and Table 4 lists their average maximum loads. The experimental maximum compressive loads of the 'with grid 60' and the 'with grid 90' specimens were 2.2 and 2.6 times larger than those of the 'without grid 60' and the 'without grid 90' specimens, respectively. Moreover, the experimental maximum compressive loads of the 'with grid' specimens were larger than the sum of the maximum values of the 'without grid' and the 'grid alone' specimens. These facts showed the reinforcement effect of the grids on CFRP cylindrical shells.

Figure 16 shows the comparison of the specific strength η calculated from the following equation.

$$\eta = \frac{\text{Maximumload (kN)}}{\text{Weight (N)}} \tag{1}$$

The η values of the 'with grid 60' and the 'with grid 90' specimens were 1.6 and 1.9 times larger than those of the 'without grid 60' and the 'without grid 90' specimens, respectively. From the view point of the specific strength, the isogrid stiffeners were effective for the reinforcement of the CFRP cylindrical shells

4.2. Fracture aspect

In the 'with grid 60' specimen, the local buckling took place at the surface skin surrounded by the stiffeners (Figure 17) and this local buckling was agreed with the FEM results shown in Figure 2. Since there were no stiffeners, the local buckling mode and the maximum load in the 'without grid 60' specimen became larger (Figure 18(a)) and smaller compared with the corresponding values of the 'with grid 60' specimen. Both the 'with grid 60' and the 'without grid 60'specimens recovered the original shape after the unloading, as shown in Figure 18(b), due to an elastic buckling.

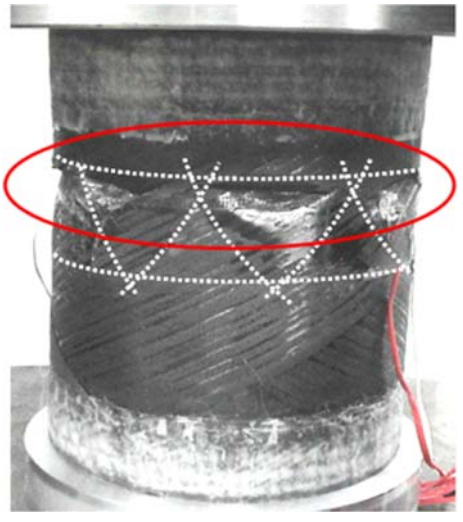

Figure 17. Failure mode of the ‘with grid 60’ specimen.

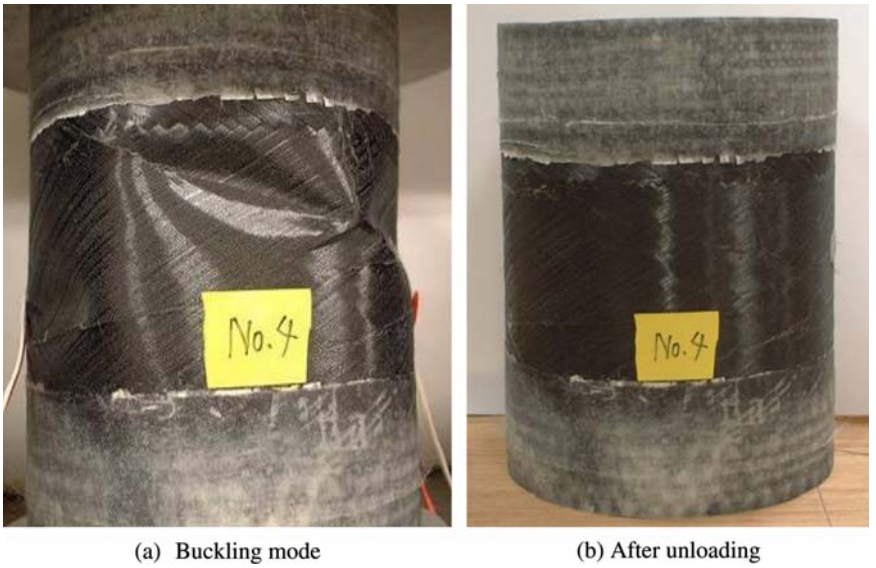

(a) Buckling mode (b) After unloading

Figure 18. Failure mode of the ‘without grid 60’ specimen.

Figures 19 and 20 show the failure aspects of the ‘with grid 90’ and the ‘without grid 90’specimen. The ‘with grid 90’ specimen presented the failure at the offset parts and the crack occurred on the surface skin along the hoop direction. In the ‘without grid 90’ specimen, the crack occurred on the surface skin along the hoop direction. In the experimental results of load to displacement for the ‘with grid 90’ specimens, as shown in Figure 14, the material fracture at the offset parts took place at the maximum load of about 40 kN and the maximum load dropped to the somewhat lower value than the maximum load of the ‘without grid 90’ specimens because the failure of the surface skins did not yet occur.

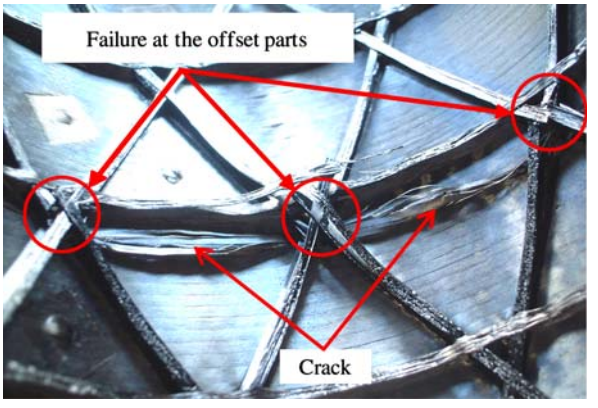

Figure 19. Failure aspect of the 'with grid 90' specimen.

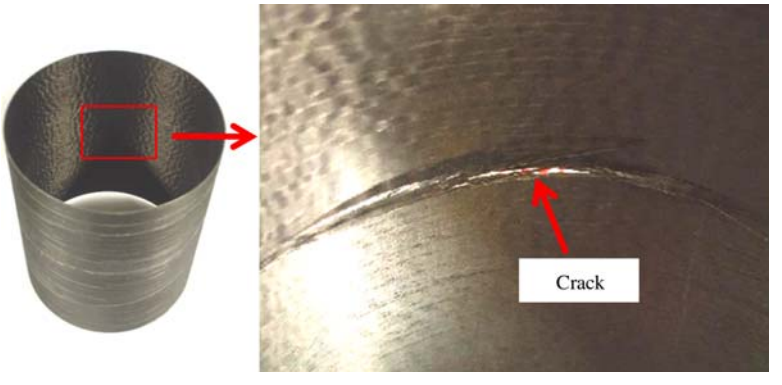

Figure 20. Failure aspect of the 'without grid 90' specimen.

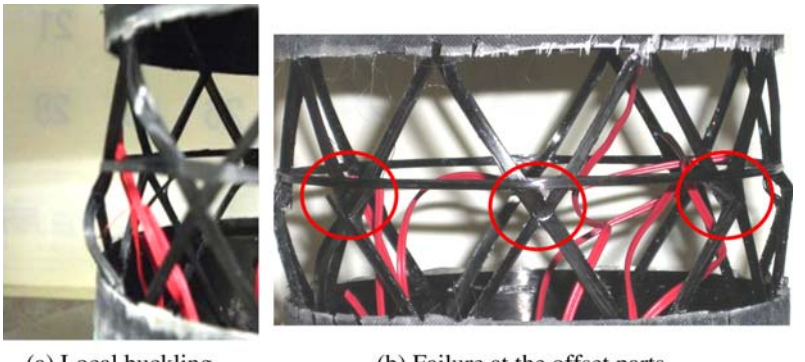

Figure 21. Failure mode of the 'grid alone' specimen.

Figure 21 shows the failure aspects of the 'grid alone' specimen. The local buckling took place at the helical stiffener. After the buckling, the failure occurred at the offset parts.

Table 5. Comparison between experimental and the FEM results.

	Experiment (kN)	FEM (Linear buckling load) (kN)	Difference (%)
Without grid 60	13.9	35.8	61.2
Without grid 90	14.5	34.3	57.7
With grid 60	30.7	86.6	64.5
With grid 90	37.8	109.3	65.4
Grid alone	9.6	23.5	59.1

4.3. Discussion

Table 5 lists the comparison between experimental and FEM results. The experimental values were smaller than the FEM ones. Considering the effect of the initial imperfections on the buckling load, the experimental values almost agreed with the conventional ones [12].

According to the results of the buckling loads calculated from the analytical formula and the linear buckling loads obtained by the eigen value analysis, the local buckling loads, the global buckling loads obtained by the nonlinear analysis, and the material failure loads based on the Tsai–Wu criterion [13,14], the experimental value of the 'with grid 90' was smaller than the local buckling load and the material failure load. Since the local buckling load was larger than the material failure load, the 'with grid 90' seemed to be the material failure, not the buckling failure. On the other hand, the buckling load of the 'with grid 60' was smaller than the material failure load and it was closer to the experimental value than the material failure load. So, the buckling failure seemed to occur in the 'with grid 60'. However, the effect of delamination between the surface skin and the grid stiffeners was not discussed in these numerical analyses. In order to obtain closer agreement and the actual strength of the CFRP isogrid cylindrical shells, the numerical analysis of the CFRP isogrid cylindrical shells with the delamination will be carried out in the future work.

5. Conclusions

1. The CFRP isogrid cylindrical shells were fabricated with the three-axes filament winding apparatus. By using the parallelogram shape of the silicone rubber female mold, the CFRP isogrid cylindrical shells could be fabricated with smaller effect of the seam line.
2. The axial compressive tests were carried out and verified the reinforcement effect of the grids on the CFRP cylindrical shells. The maximum loads of the CFRP isogrid cylindrical shells were larger than the sum maximum values of the CFRP cylindrical shells and the grid alone.
3. The specific strength η values of the 'with grid 60' and the 'with grid 90' specimens were 1.6 and 1.9 times larger than those of the 'without grid 60' and the 'without grid 90' specimens, respectively. These facts also demonstrated the reinforcement effect of the grids on the CFRP cylindrical shells.

References

[1] Fukushima Y, Shimizu R, Kajiura K, Nishi T. The structure of H-II A Rocket. Aeronaut. Space Sci. Jpn. 1998;50:10–15.
[2] Vasiliev VV, Barynin VA, Rasin AF. Anisogrid lattice structures – survey of development and application. Compos. Struct. 2001;54:361–370.
[3] Huybrechts SM, Meink TE, Wegner PM, Granley JM. Manufacturing theory for advanced grid stiffened structures. Compos. A. 2002;33:155–161.

[4] Kidane S, Li G, Helms J, Pang SS, Woldesenbet E. Buckling load analysis of grid stiffened composite cylinders. Compos. B. 2003;34:1–9.
[5] Chen Y, Gibson RF. Analytical and experimental studies of composite isogrid structures with integral passive damping. Mech. Adv. Mater. Struct. 2003;10:127–143.
[6] Higgins J, West BV. NDE and repair of damaged Minotaur fairing shell. Compos. Struct. 2005;67:189–195.
[7] Vasiliev VV, Razin AF. Anisogrid composite lattice structures for spacecraft and aircraft applications. Compos. Struct. 2006;76:182–189.
[8] Shirinzadeh B, Alici G, Foong CW, Cassidy G. Fabrication process of open surfaces by robotic fiber placement. Rob. Computer-Integr. Manuf. 2004;20:17–28.
[9] Lopes CS, Gurdal Z, Camanho PP. Variable-stiffness composite panels: buckling and first-ply failure improvements over straight-fiber laminates. Compos. Struct. 2008;86:897–907.
[10] Kim TD. Fabrication and testing of composite isogrid stiffened cylinder. Compos. Struct. 1999;45:1–6.
[11] Kim TD. Fabrication and testing of thin composite stiffened panel. Compos. Struct. 2000;49:21–25.
[12] Hayashi T. Theory and application of light weight structures. Tokyo: Nikkagiren; 1966. p. 315–329.
[13] Ben G, Sao S, Kishitani N. Nonlinear buckling analysis of CFRP isogrid cylindrical shells. Proceedings of the 15th International Congress on Sound and Vibration (ICSV15). Korea: Daejeon; 2008. 1530–1537.
[14] Ben G, Kishitani N, Mochizuki Y. Buckling analysis and optimum design of CFRP isogrid cylindrical shells. Proceedings of the 16th International Conference on Composite Structures (ICCS-16). Portugal: Porto; 2011.